

Supplementary Information

Arrayed Silk Fibroin for High-performance Li Metal Battery and Atomic Interface Structure Revealed by Cryo-TEM

Baolin Zhang,¹ Haodong Shi,² Zhijin Ju,¹ Kai Huang,³ Cheng Lian,³ Yao Wang,¹ Ouwei Sheng,¹ Jianhui Zheng,¹ Jianwei Nai,¹ Tiefeng Liu,¹ Yang Jin,⁴ Yujing Liu,^{1*}Chuanfang (John)Zhang^{5*} and Xinyong Tao ^{1*}

¹. College of Materials science and Engineering, Zhejiang University of Technology, Hangzhou 310014, China.

². State Key Laboratory of Catalysis, Dalian Institute of Chemical Physics, Chinese Academy of Sciences, 457 Zhongshan Road, Dalian 116023, China, and University of Chinese Academy of Sciences, 19 A Yuquan Rd, Shijingshan District, Beijing 100049, China.

³. State Key Laboratory of Chemical Engineering, Frontiers Science Center for Materiobiology and Dynamic Chemistry, Shanghai Engineering Research Center of Hierarchical Nanomaterials, and School of Chemistry and Molecular Engineering, East China University of Science and Technology, Shanghai 200237, China

⁴. School of Electrical Engineering, Zhengzhou University, Zhengzhou 450001, P.R. China.

⁵. Swiss Federal Laboratories for Materials Science and Technology (Empa), ETHDomain, Überlandstrasse 129, CH-8600, Dübendorf, Switzerland.

*To whom correspondence should be addressed.

E-mail: tao@zjut.edu.cn, yujingliu@zjut.edu.cn, chuanfang.zhang@empa.ch

Supplementary Figures

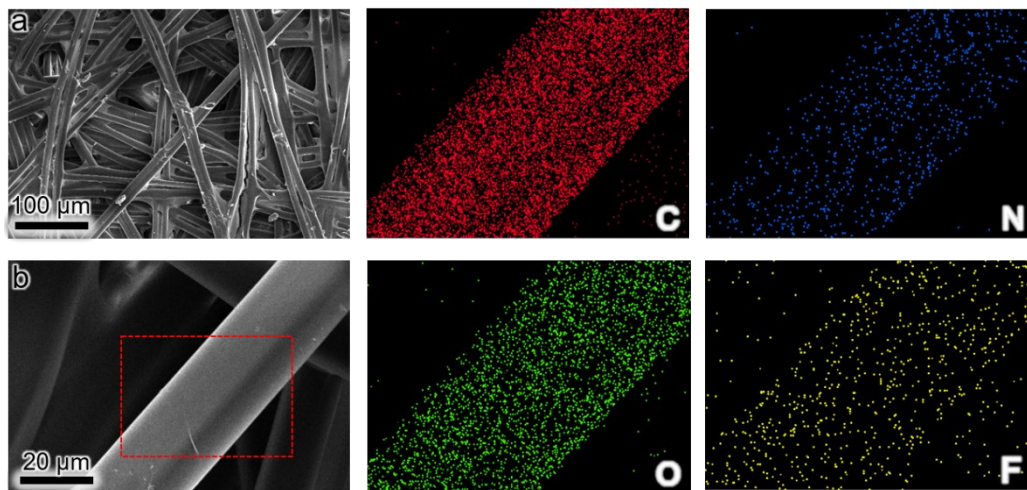


Fig. S1 Characterization of silk fibroin (SF) matrix from the top view. (a) Scanning electron microscopy (SEM) images of SF matrix. (b) SEM image of single fiber in SF matrix the corresponding elemental mapping of C, N, O, and F.

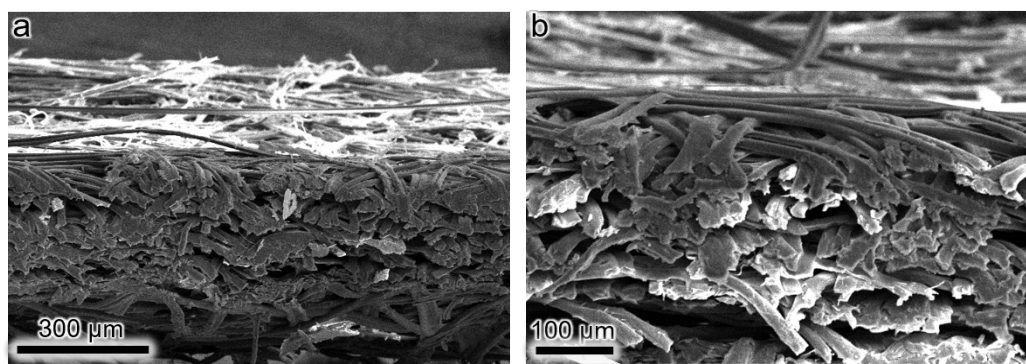


Fig. S2 Characterization of SF matrix from the cross-section view. SEM images of (a) cross-sectional SF and (b) its corresponding enlarged area.

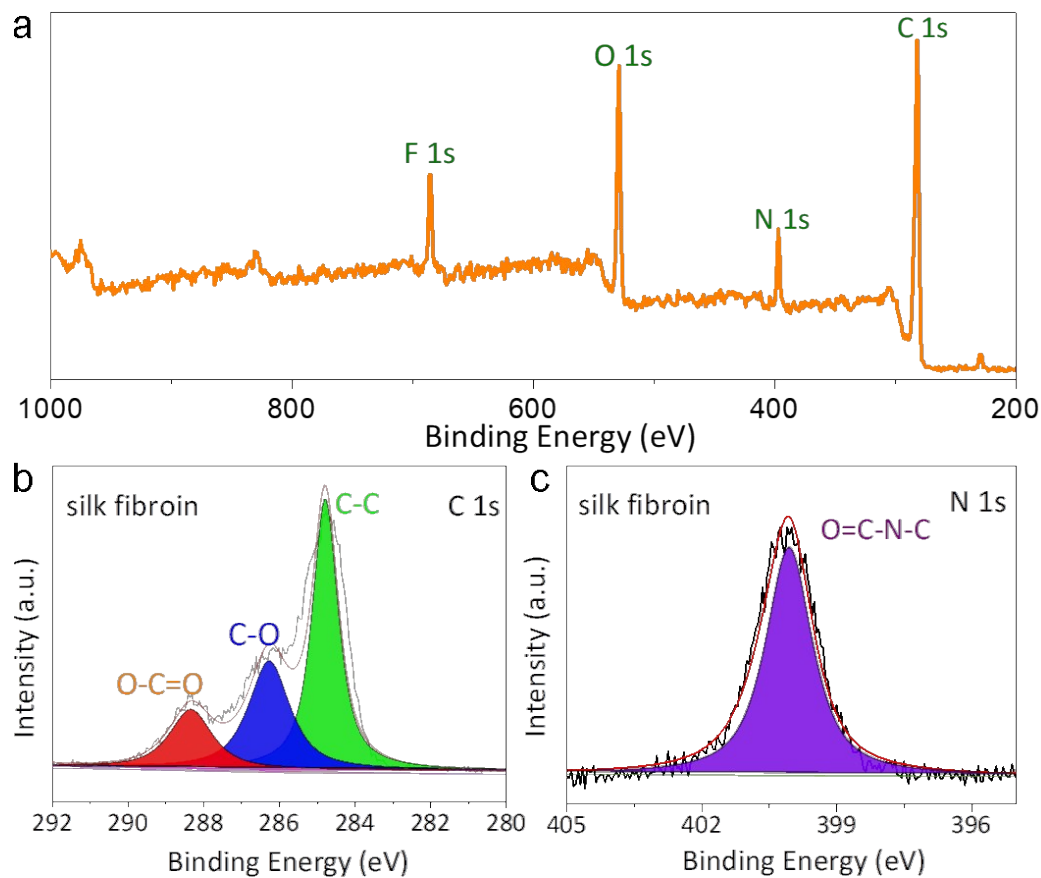


Fig. S3 XPS characterization of SF matrix. (a) XPS survey of the as-achieved SF matrix, showing the presence of F, O, N and C. (b) N 1s. (c) C 1s spectra and their deconvolution.

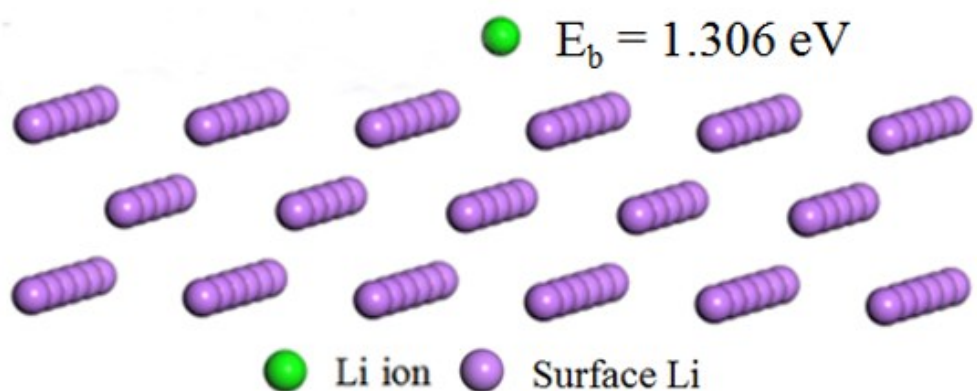


Fig. S4 The energies of Li ions and the Li(200) surface without peptide chains.

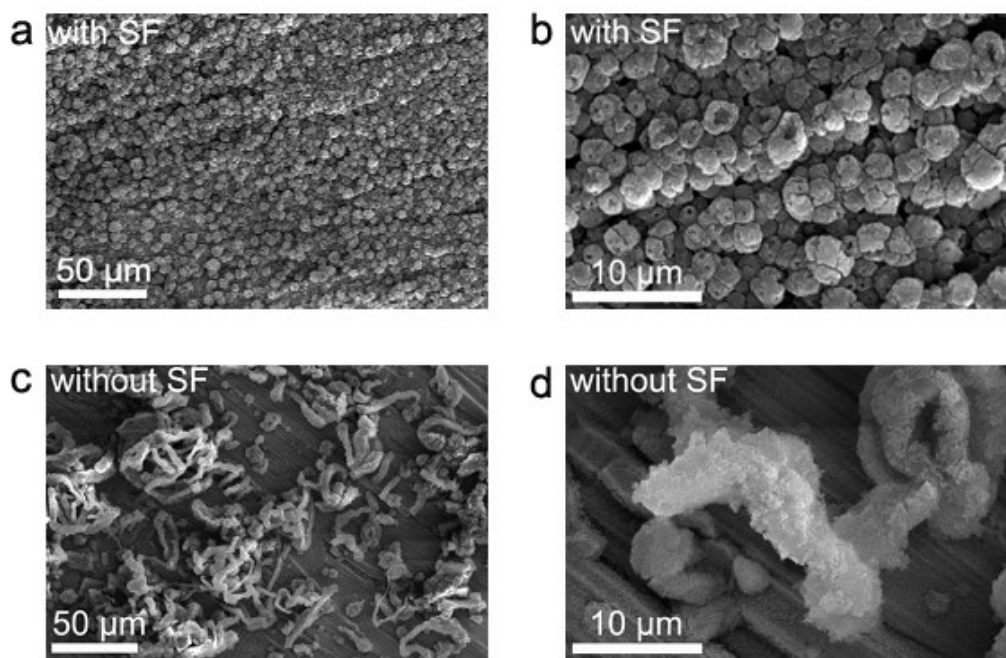


Fig. S5 SEM images in different magnification of Li deposits (a, b) with and (c, d) without SF at a current density of 0.5 mA cm^{-2} with a capacity of 0.1 mAh cm^{-2} in carbonate-based electrolytes.

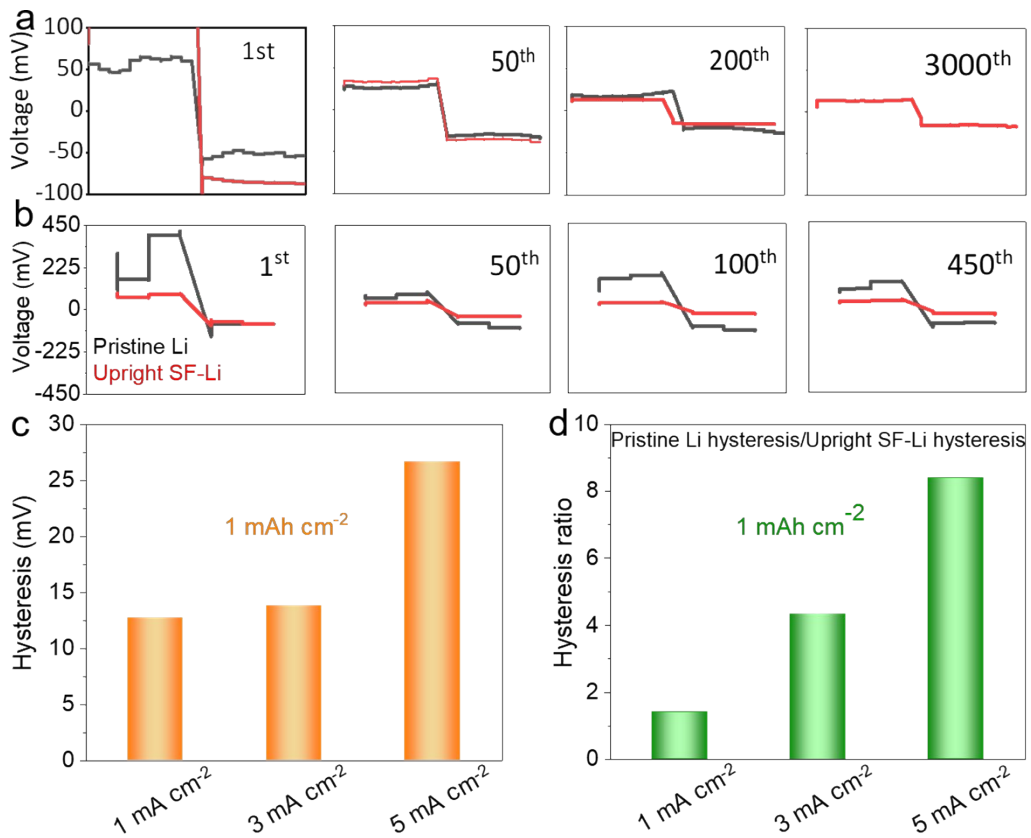


Fig. S6 Voltage hysteresis of two cells at different current densities. Enlarged voltage hysteresis at different cycling times at (a) 1.0 mA cm^{-2} and (b) 5.0 mA cm^{-2} . The Li deposition capacity was fixed to 1.0 mAh cm^{-2} . (c) the hysteresis of different current density at 1.0 mAh cm^{-2} when the pristine Li-based symmetric cell was stabilized. (d) Ratio of the voltage hysteresis of pristine Li symmetric cell to the upright SF-Li based cell at different current densities at 1.0 mAh cm^{-2} when the cells were stabilized.

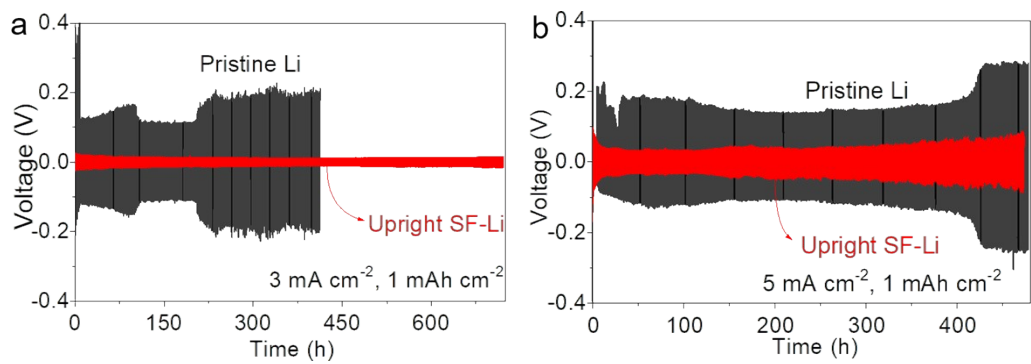


Fig. S7 Electrochemical performance comparison of cells based on pristine Li foil and upright SF-Li anode. Voltage profiles comparison under a current density of (a) 3 mA cm^{-2} and (b) 5 mA cm^{-2} with a cycling capacity of 1 mAh cm^{-2} .

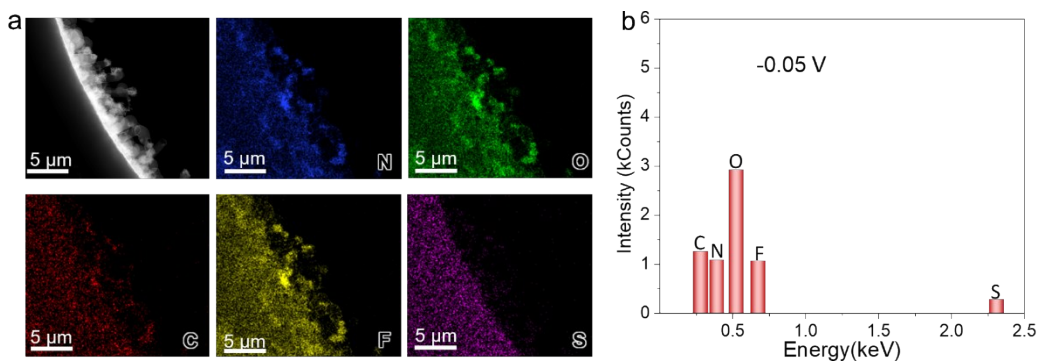


Fig. S8 Cryo-TEM mapping images of Li deposited on the bare Cu grids, showing non-uniform Li deposition and growth of dendrites are clearly visible at -0.05 V in ether-based electrolytes at 1 mA cm⁻² with a capacity of 0.5 mAh cm⁻². (a). The needle-like dendrites from the N, O, C, F and S mapping images also indicate that SEI layer cover the as-deposited Li. (b) The spectrum of element intensity obtained from (a).

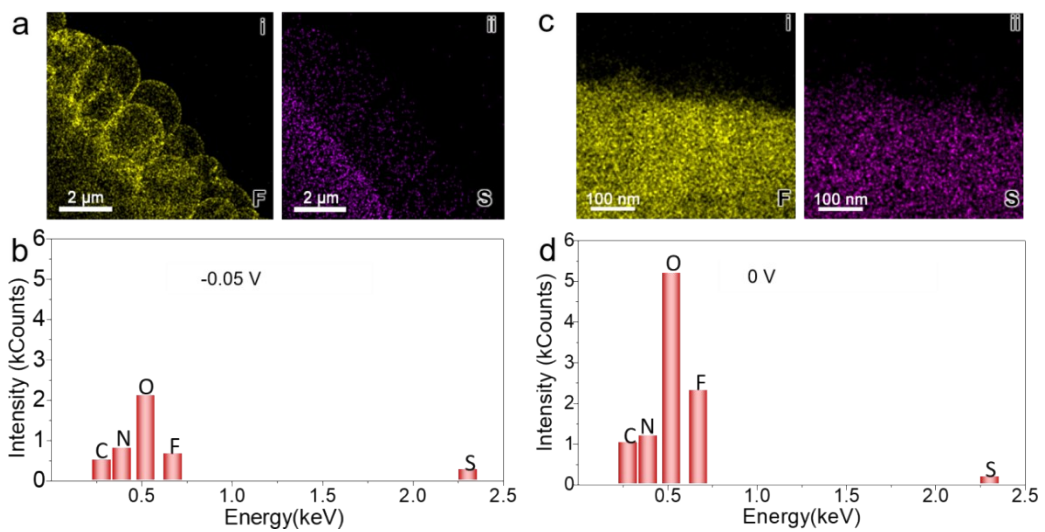


Fig. S9 (a) The effect of SF on the Li plating revealed by the cryo-TEM images via elemental mapping, showing uniform distribution of F and S signals in the spherical Li nuclei at -0.05 V. (b) the spectrum of element intensity obtained from the cryo-TEM element mapping. (c) cryo-TEM elemental mapping images of SF-containing system at 0 V, showing SF partially dissolves into the electrolyte and participate the SEI formation, as indicated by the uniform distribution of F and S. (d) the spectrum of element intensity obtained from the cryo-TEM element mapping.

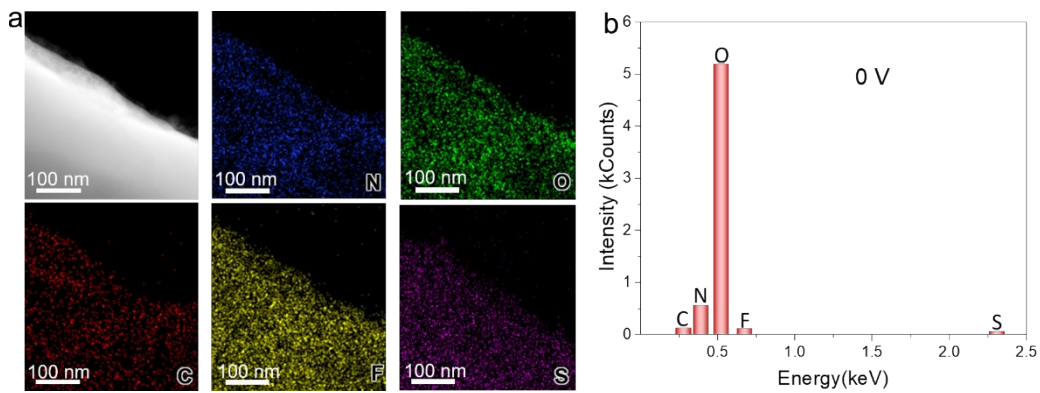


Fig. S10 Cryo-TEM mapping images on the bare Cu grids upon SEI formation when SF is absent. (a). The growth of SEI layer was conducted at 0 V in ether-based electrolytes at 0.05 mA cm^{-2} . (b) The spectrum of element intensity obtained from cryo-TEM EDX element analysis.

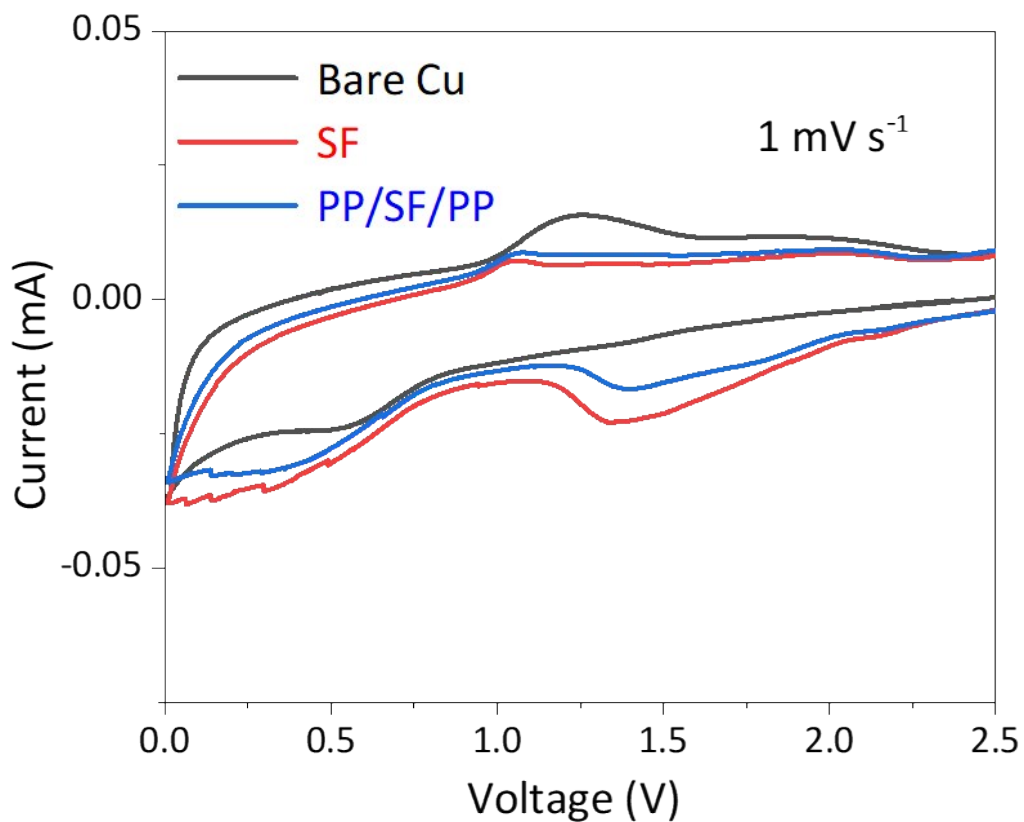


Fig. S11 Cyclic voltammetry of half cells based on bare Cu, SF, and SF insulated by double-layer polypropylene (PP), respectively at a scan rate of 1 mV s^{-1} in ether-based electrolytes. The larger integrated area in the SF-based cell suggest SF participates the electrochemical redox reaction occurring at 1.5 V.

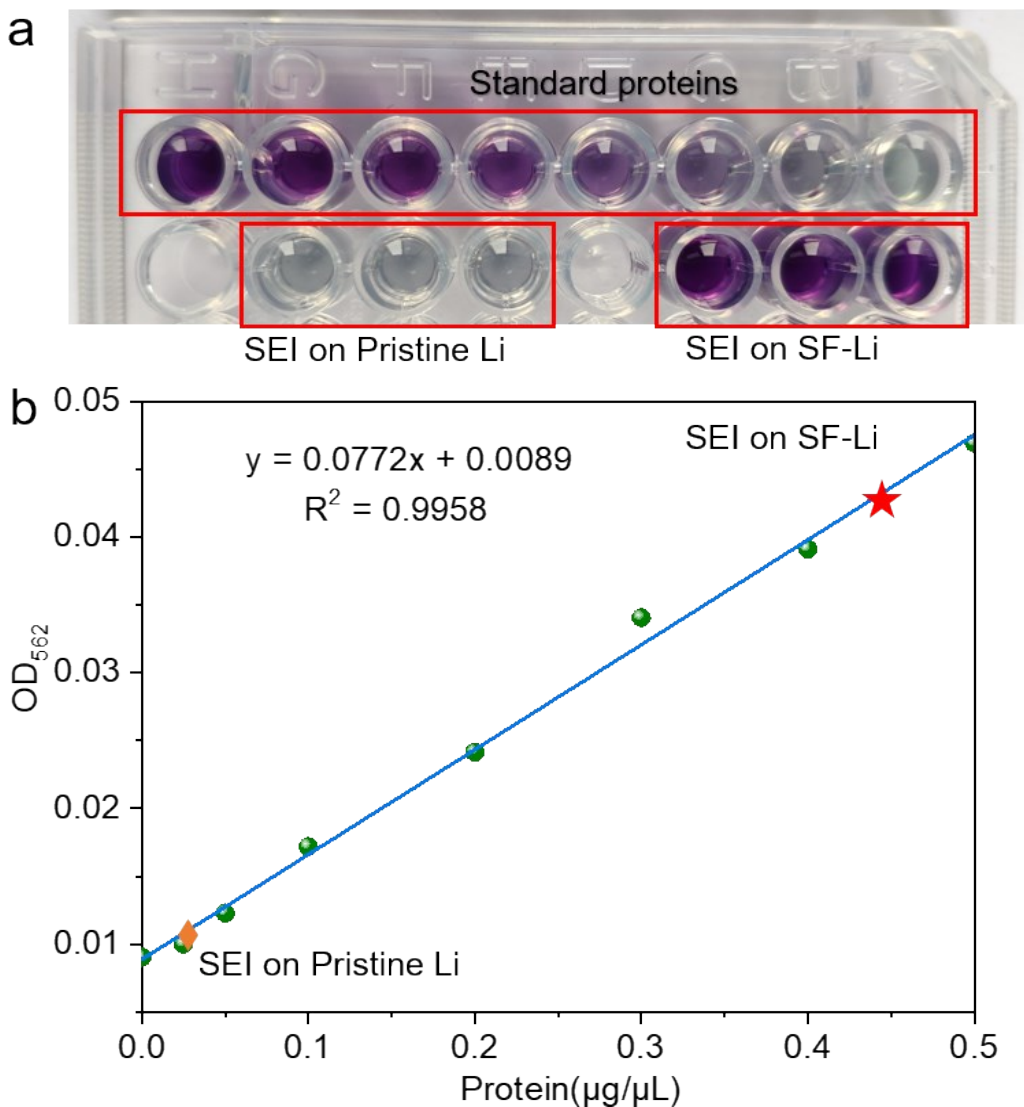


Fig. S12 BCA protein assay for SEI on SF-Li anode. (a) The BCA assay showing the typical chromogenic reaction of standard proteins, SEI on SF-Li anode, and SEI on pristine Li in BCA reagent. The color of standard sample changes from light grey to deep purple as the protein concentration increases. (b) The curve of the absorbance at 562 nm vs protein concentration is plotted by the standard protein sample in (a), where the protein concentrations of the SEI on SF-Li anode or pristine Li are highlighted (The protein concentration of SEI on SF-Li anode is 0.424 $\mu\text{g}/\mu\text{L}$ and the SEI on pristine Li did not contain protein within the error range).

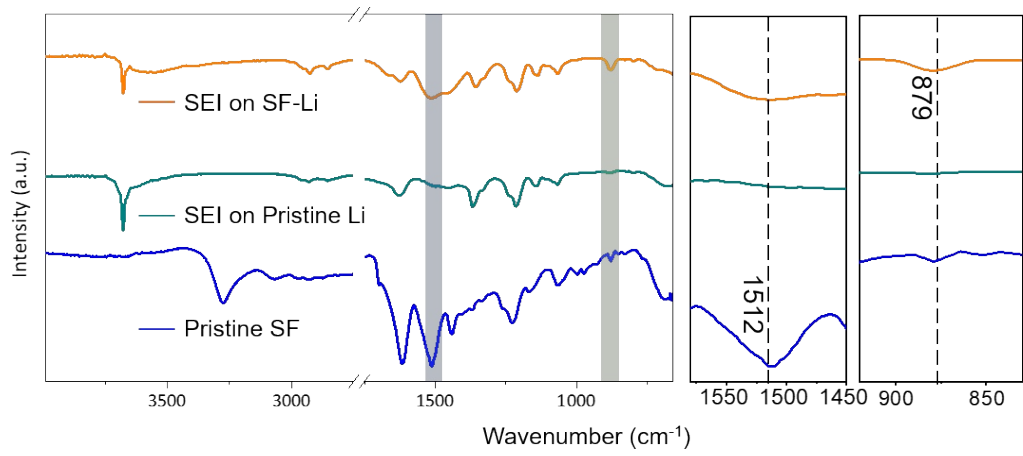


Fig. S13 FTIR spectra of the pristine SF, SEI on SF-Li anode, and SEI on pristine Li after 20 cycles at 2 mA cm^{-2} with 1 mAh cm^{-2} in ether-based electrolytes. The peaks at 1512 and 879 cm^{-1} indicate the presence of in-plane N-H bending and out-of-plane N-H bending.

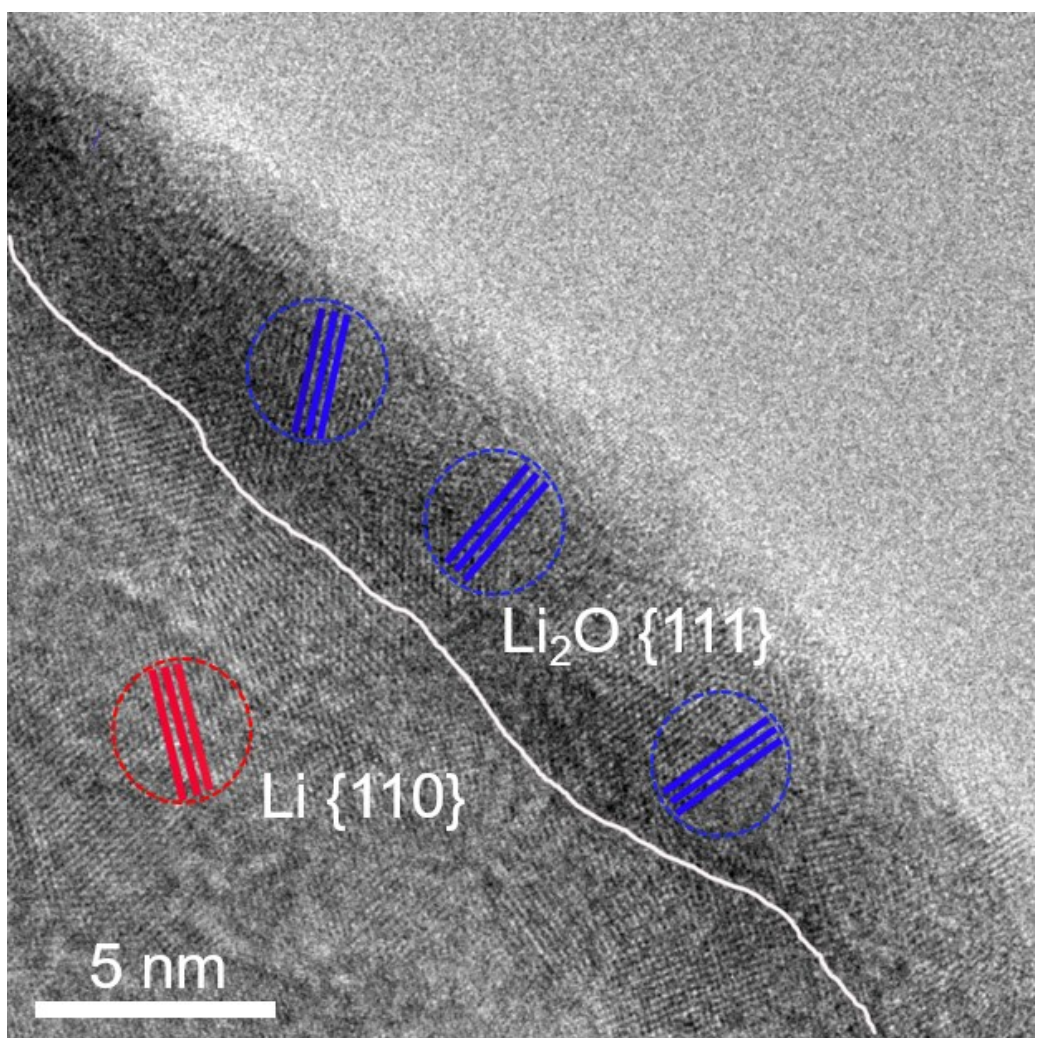


Fig. S14 The conventional mosaic SEI in the Li deposited on the simple SF-containing Cu grid.

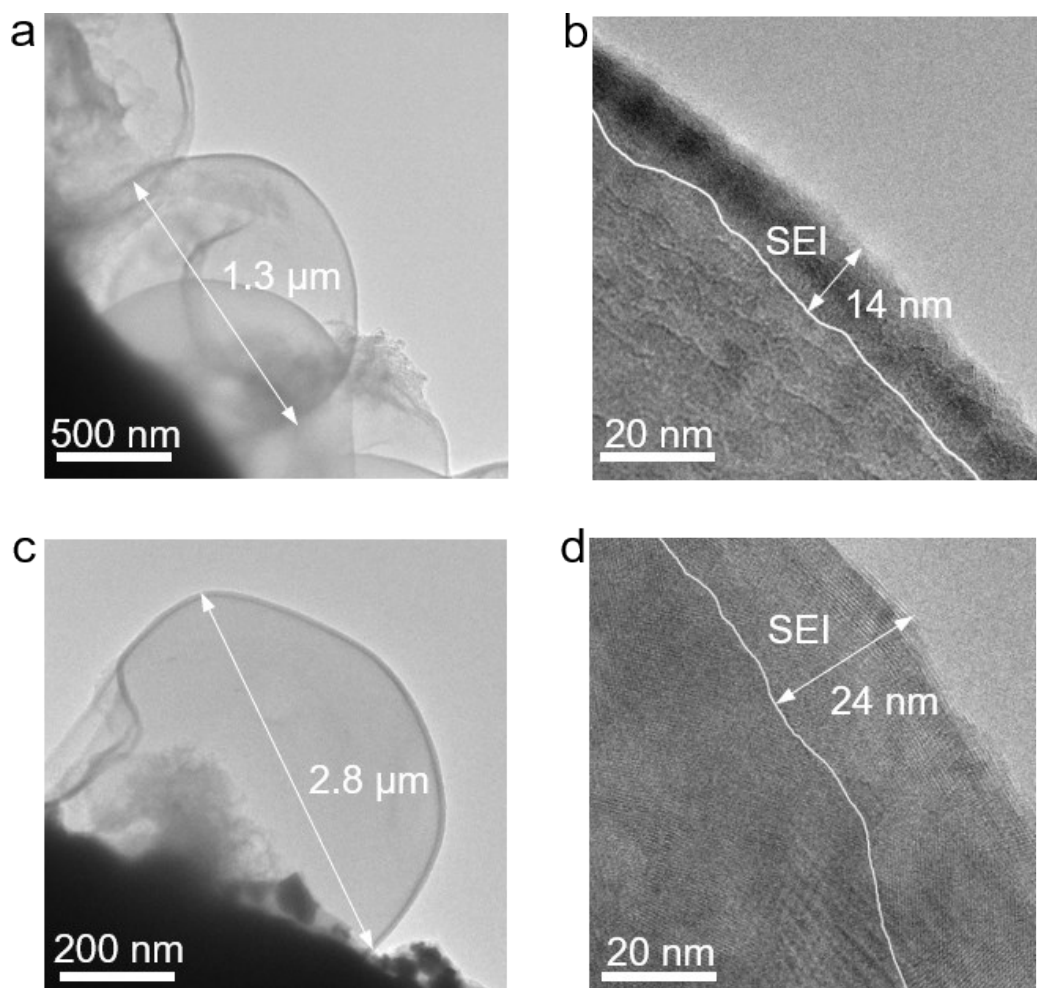


Fig. S15 Cryo-TEM reveals an emergent SEI nanostructure formed at different test method. (a,b) Li metal was deposited onto a Cu grid in DOL/DME/LiNO₃ electrolyte using 1 M LiTFSI salt. (c,d) The growth behavior of Li inside the SF-Li upright structure. (a,c) cryo-EM images of Li metal particles showing the particle size. (b,d) cryo-TEM images of the SEI interface showing the SEI thickness.

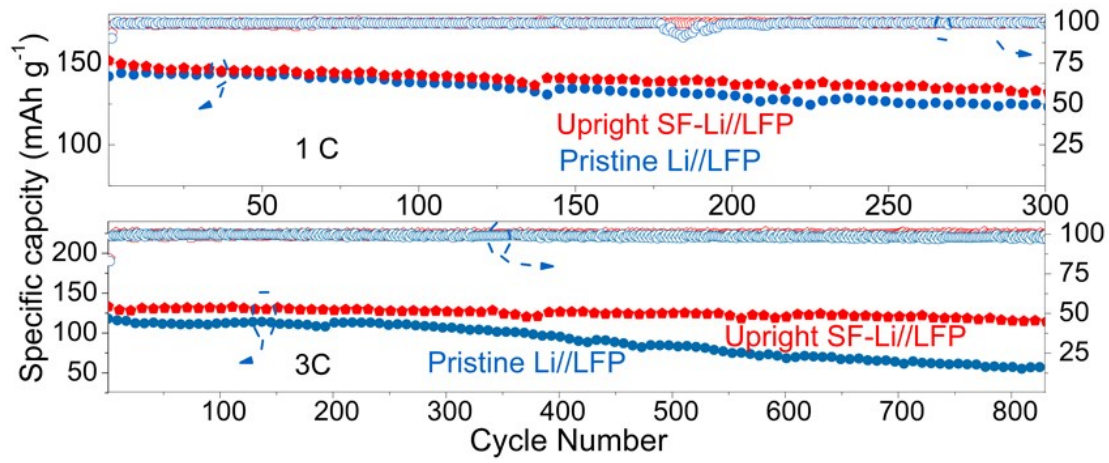


Fig. S16 Electrochemical performance of cells based on the upright SF-Li anode pairing with LFP cathode in presence of the ether-based electrolyte.

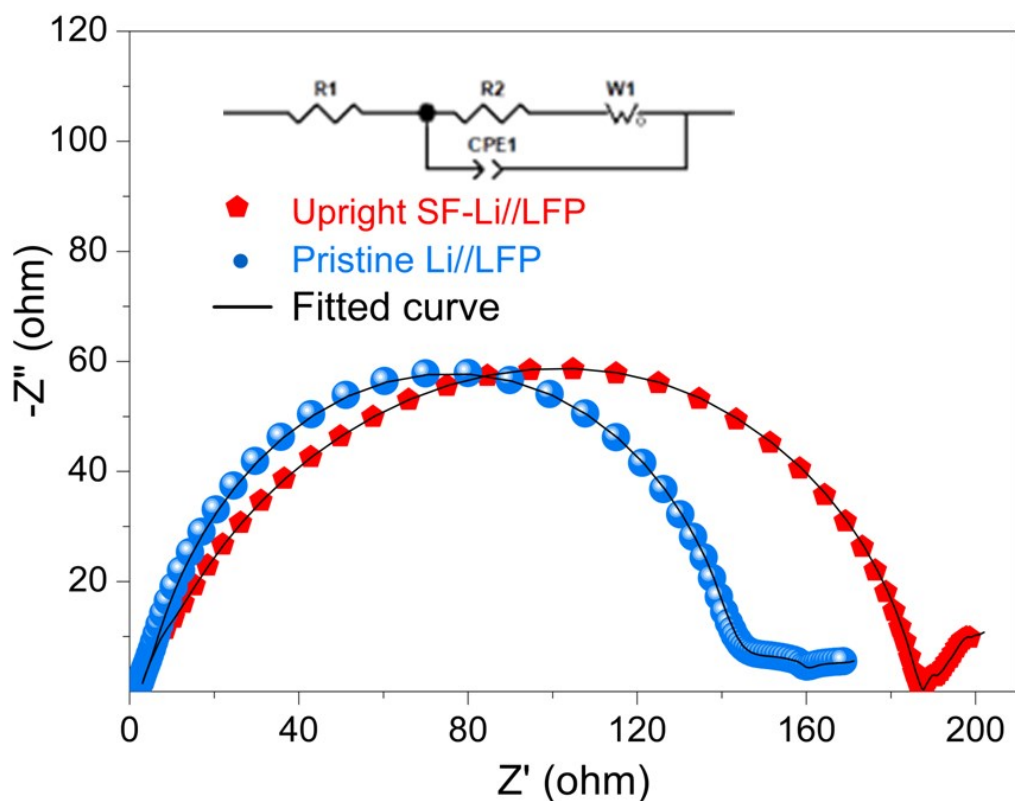


Fig. S17 Nyquist plots of two full cells before cycling.

Supplementary Tables

Table S1. Galvanostatic cycling performance of upright SF-Li anode compared with other state-of-the-art Li metal composite anodes.

Current /Capacity (mA cm ⁻² / mAh cm ⁻²)	Lifespan (h / cycle)	Hysteresis (mV)	Strategy	Reference
1 / 1	1450 / 725	25	3D@Al@Li	1
	850 / 425	12	BGCF@Li	2
	1600 / 800	48	Mn/G@Li	3
	500 / 250	50	3D Li/Ni	4
	3200 / 1475	14	Upright SF-Li	This work
3 / 1	120/180	300	CF-Li	5
	670 / 1000	100	q-PET host	6
	100 / 150	50	Li@10Alucone	7
	133 / 200	150	carbonized wood	8
	720 / 1080	15	Upright SF-Li	This work
5 / 1	80 / 200	50	PMF foam	9
	84 /210	200	ZnO-/CNT-coated-Li	10
	130 / 325	160	GZCNT interfacial layer	11
	40 / 100	125	OIFN film	12
	500 / 1250	35	Upright SF-Li	This work

Table S2. The relevant atomic and mass fraction of various elements upon Li plating measured through EDX elemental analysis with SF a), and without SF b) on the Cu grids supported on the Cu foil.

a		b			
Atomic fraction ratio		Mass fraction ratio			
N/C: 1.05		N/C: 1.23			
O/C: 21.97		O/C: 29.24			
Element	Atomic fraction(%)	Mass fraction(%)	Element		
N	4.25867	3.74897	N	4.06949	3.61148
F	2.41877	2.88811	F	2.75755	3.31932
O	88.7496	89.2427	O	85.7718	86.9474
S	0.53020	1.06849	S	0.38533	0.78283
C	4.04277	3.05175	C	7.01582	5.33893

Table S3. The relevant atomic and mass fraction of various elements upon SEI formation measured through EDX elemental analysis with SF a) and without SF b) on the Cu grids supported on the Cu foil.

a		b			
Atomic fraction ratio	Mass fraction ratio	Atomic fraction ratio	Mass fraction ratio		
N/C: 0.86	N/C: 1.00	N/C: 0.25	N/C: 0.30		
O/C: 6.86	O/C: 9.14	O/C: 1.68	O/C: 2.24		
Element	Atomic fraction(%)	Mass fraction(%)	Element		
N	8.17716	7.15234	N	7.07846	6.43251
F	16.8209	19.9562	F	17.2489	21.2610
O	65.1805	65.1225	O	46.8279	48.6087
S	0.32150	0.64377	S	0.93811	1.95161
C	9.49996	7.12525	C	27.9067	21.7462

Table S4. EIS simulation results from Figure 5e and Figure S16

Battery	Before cycling		After 150 cycles		
	sample	$R_s(\Omega)$	$R_f(\Omega)$	$R_s(\Omega)$	$R_f(\Omega)$
Pristine Li//LFP		6.154	36.7	4.502	73.44
Upright SF-Li//LFP		10.081	191.4	6.033	37.66

Table S5. The capacity and cycling lifespan of the upright SF-Li//LFP cell compared with other state-of-the-art Li metal composite //LFP cell.

Current density	Cathode loading(mg cm ⁻²)	Electrolyte Type	Cycling Time (h)	Capacity retention	Strategy	Reference
1C	10	Carbonate electrolyte	700	78	CP-NCNS-Li	¹³
1C	12.5	Ether-based Electrolyte	500	90.5	LCNM-Ni-Li	¹⁴
1C	10.45	Carbonate electrolyte	600	99	SR-G-Li	¹⁵
4C	7.85	Carbonate electrolyte	300	76.3	3DCP-Li	¹⁶
2C	3.55	Carbonate electrolyte	500	90	CF-Li	¹⁷
1C	5	Carbonate electrolyte	1600	93	Upright SF-Li	This work

References

- 1 H. Ye, Z.-J. Zheng, H.-R. Yao, S.-C. Liu, T.-T. Zuo, X.-W. Wu, Y.-X. Yin, N.-W. Li, J.-J. Gu, F.-F. Cao and Y.-G. Guo, *Angew. Chem., Int. Ed.*, 2019, **58**, 1094-1099.
- 2 H. Duan, J. Zhang, X. Chen, X.-D. Zhang, J.-Y. Li, L.-B. Huang, X. Zhang, J.-L. Shi, Y.-X. Yin, Q. Zhang, Y.-G. Guo, L. Jiang and L.-J. Wan, *J. Am. Chem. Soc.*, 2018, **140**, 18051-18057.
- 3 B. Yu, T. Tao, S. Mateti, S. Lu and Y. Chen, *Adv. Funct. Mater.*, 2018, **28**, 1803023.
- 4 L. Yu, N. L. Canfield, S. Chen, H. Lee, X. Ren, M. H. Engelhard, Q. Li, J. Liu, W. Xu and J.-G. Zhang, *ChemElectroChem*, 2018, **5**, 761-769.
- 5 Y. Zhang, C. Wang, G. Pastel, Y. Kuang, H. Xie, Y. Li, B. Liu, W. Luo, C. Chen and L. Hu, *Adv. Energy Mater.*, 2018, **8**, 1800635.
- 6 W. Zhang, H. L. Zhuang, L. Fan, L. Gao and Y. Lu, *Sci. Adv.*, 2018, **4**, eaar4410-eaar4410.
- 7 Y. Zhao, L. V. Goncharova, Q. Sun, X. Li, A. Lushington, B. Wang, R. Li, F. Dai, M. Cai and X. Sun, *Small Methods*, 2018, **2**, 1700417.
- 8 Y. Zhang, W. Luo, C. Wang, Y. Li, C. Chen, J. Song, J. Dai, E. M. Hitz, S. Xu, C. Yang, Y. Wang and L. Hu, *Proc. Natl. Acad. Sci. USA*, 2017, **114**, 3584-3589.
- 9 L. Fan, H. L. Zhuang, W. Zhang, Y. Fu, Z. Liao and Y. Lu, *Adv. Energy Mater.*, 2018, **8**, 1703360.
- 10 H. Zhang, X. Liao, Y. Guan, Y. Xiang, M. Li, W. Zhang, X. Zhu, H. Ming, L. Lu, J. Qiu, Y. Huang, G. Cao, Y. Yang, L. Mai, Y. Zhao and H. Zhang, *Nat. Commun.*, 2018, **9**, 3729.
- 11 H. Zhang, X. Liao, Y. Guan, Y. Xiang, M. Li, W. Zhang, X. Zhu, H. Ming, L. Lu, J. Qiu, Y. Huang, G. Cao, Y. Yang, L. Mai, Y. Zhao and H. Zhang, *Nat. Commun.*, 2018, **9**, 3729-3729.
- 12 S. Liu, X. Xia, S. Deng, D. Xie, Z. Yao, L. Zhang, S. Zhang, X. Wang and J. Tu, *Adv. Mater.*, 2019, **31**, 1806470.
- 13 Y. Zhao, X. Yang, Q. Sun, X. Gao, X. Lin, C. Wang, F. Zhao, Y. Sun, K. R. Adair, R. Li, M. Cai and X. Sun, *Energy Storage Materials*, 2018, **15**, 415-421.
- 14 L. Liu, Y.-X. Yin, J.-Y. Li, Y.-G. Guo and L.-J. Wan, *Chemical Communications*, 2018, **54**, 5330-5333.
- 15 M. Bai, K. Xie, K. Yuan, K. Zhang, N. Li, C. Shen, Y. Lai, R. Vajtai, P. Ajayan and B. Wei, *Advanced Materials*, 2018, **30**, 1801213.
- 16 X. Zhou, W. Huang, C. Shi, K. Wang, R. Zhang, J. Guo, Y. Wen, S. Zhang, Q. Wang, L. Huang, J. Li, X. Zhou and S. Sun, *ACS Applied Materials & Interfaces*, 2018, **10**, 35296-35305.
- 17 Y. Zhang, C. Wang, G. Pastel, Y. Kuang, H. Xie, Y. Li, B. Liu, W. Luo, C. Chen and L. Hu, *Advanced Energy Materials*, 2018, **8**, 1800635.